JACS
JOURNAL OF THE AMERICAN CHEMICAL SOCIETY

Communication

pubs.acs.org/JACS

Binary Protein Crystals for the Assembly of Inorganic Nanoparticle Superlattices

Matthias Künzle,[†] Thomas Eckert,[‡] and Tobias Beck*[,†]

[†]Institute of Inorganic Chemistry, RWTH Aachen University, 52074 Aachen, Germany
[‡]Institute of Physical Chemistry, RWTH Aachen University, 52074 Aachen, Germany

Supporting Information

ABSTRACT: Biomolecules can act as functional templates for the organization of inorganic particles. Here we use two protein containers, engineered with opposite surface charge, as building blocks for the construction of a new type of biohybrid material. Binary structures with crystalline order were obtained, adopting a tetragonal lattice. Moreover, the cavity of the engineered protein containers can be filled with inorganic nanoparticles. The controlled assembly of these protein−nanoparticle composites yields highly ordered binary nanoparticle superlattices as free-standing crystals, with up to a few hundred micrometers in size. Because the structure and lattice parameters of the protein−nanoparticle crystals are independent of their nanoparticle cargo, the binary protein material may serve as a generally applicable matrix for the assembly of a variety of nanoparticles types.

Structural and functional diversity of biomolecules, such as proteins or DNA, can be combined with the unique properties of nanoparticles, to realize new biohybrid materials with tunable physical and chemical properties.[1−3] Typically, most work has focused on the assembly of oligonucleotide-functionalized nanoparticles into crystalline superlattices.[4,5] These highly sophisticated approaches can organize various nanoparticle types and produce binary and ternary systems with tailorable crystal lattices and lattice parameters.[6,7] In contrast, proteins have been underexploited as molecular linkers and templates for nanoparticle assembly despite their interesting chemical properties and inherent functionalities. Although there are reports on the directed assembly of proteins,[8−11] the formation of biohybrid structures composed of proteins and nanoparticles still represents a major challenge.[12−18] In general, despite important advances in fabricating a variety of different crystal structures with the help of biomolecules, the overall domain sizes remain rather small. Inhomogeneity in size and morphology of the buildings blocks hampers crystal growth and renders mesoscale or even larger structures currently elusive. Therefore, alternative approaches are required that assemble individual nanoscale building blocks into crystalline materials with high long-range order.

Here we introduce an atomically precise ligand shell based on protein containers that can overwrite any nanoparticle inhomogeneity and drastically increase the crystal assembly size in three dimensions. Moreover, by using a design approach with two complementary building blocks, we generated binary nanoparticle superlattices with two different types of nanoparticles positioned precisely within the superlattice, important for synergistic interactions within a multifunctional material.[19,20]

Protein containers present a viable building block for the construction of structured materials because they have an atomically precise shape defined by their molecular composition. A wide variety of naturally occurring protein containers are available, and recently novel artificial containers have been designed.[21,22] Protein containers offer an enormous plasticity. The protein shell can be mutated or functionalized without impeding container formation.[23−25] Moreover, the container cavity presents an attractive compartment for storage of molecules,[26] and as a reaction chamber.[27]

After introduction of charged residues on the surface of protein containers, we utilized electrostatic interactions between complementarily charged protein containers for the assembly into binary three-dimensional structures, in analogy to the formation of inorganic salts from oppositely charged ions. The container cavities can be filled with two types of nanoparticles (Figure 1).

As building block, we selected human heavy chain ferritin, a protein essential for iron mineralization and storage.[28] The

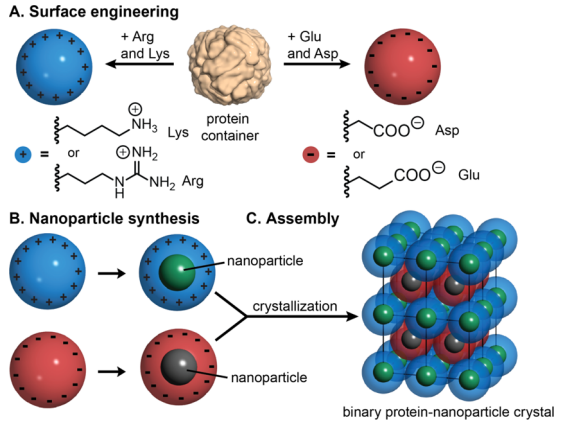

Figure 1. General scheme for the assembly of binary nanoparticle superlattices based on charged protein containers. (A) The surface of a native protein container is engineered to produce containers with a positively charged (left) and negatively charged surface (right). (B) Nanoparticle synthesis is carried out separately in each protein container type. (C) Self-assembly of the protein container nanoparticle composites yields highly ordered three-dimensional superlattices.

Received: July 13, 2016
Published: September 12, 2016

DOI: 10.1021/jacs.6b07260
J. Am. Chem. Soc. 2016, 138, 12731−12734

container is composed of 24 subunits with octahedral symmetry and has an outer diameter of ~12 nm. Ferritin has been extensively used as reaction vessel for the size-restrained synthesis of nanoparticles,[29−31] and for the encapsulation of small molecules,[32] dyes,[33] or presynthesized nanoparticles.[34]

For the negatively charged building block, we re-engineered the exterior surface of wild-type ferritin to yield the variant Ftn$^{(neg)}$, analogous to the positively charged variant Ftn$^{(pos)}$.[35] By introducing four additional glutamic acid residues per container subunit (Figure S1), a large negative net charge on the outer ferritin surface was established for strong electrostatic interaction with its cationic counterpart Ftn$^{(pos)}$. The positively charged building block Ftn$^{(pos)}$ carries nine cationic mutations per container subunit, rendering the outer container surface strongly positive (Figure 2A).

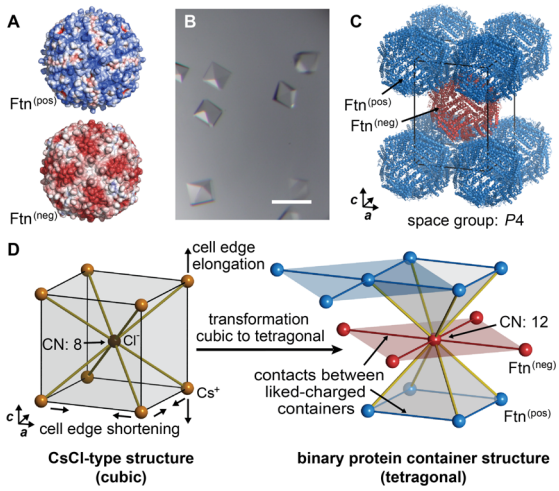

Figure 2. (A) Electrostatic potential (red, −5 kT/e; blue, +5 kT/e) of Ftn$^{(pos)}$ and Ftn$^{(neg)}$, viewed along the 4-fold axis. (B) Optical micrograph of crystals composed of Ftn$^{(pos)}$ and Ftn$^{(neg)}$, scale bar 200 μm. (C) Molecular structure of binary crystals. One unit cell of the tetragonal lattice is shown, protein backbone depicted in cartoon representation. (D) Transformation from the binary cubic CsCl-type structure (left) to the present tetragonal binary protein container structure (right), spheres not drawn to scale, CN: coordination number.

No mutations were introduced near channels or monomer interfaces to ensure that assembly and functionality of the protein containers were not impaired. The variants Ftn$^{(pos)}$ and Ftn$^{(neg)}$ could be readily produced in *E. coli* and were purified to yield highly pure samples (Figure S2).

Ordered assembly of nanoscale building blocks requires control over the assembly conditions, e.g., chemical composition, temperature, interaction strength between building blocks and development over time. We rationalized that the crystallization setup used in protein crystallography should be applicable to the assembly of complementarily charged protein containers, because it enables control over the aforementioned parameters. To this end, we first screened for suitable crystallization conditions using commercially available protein crystallization screens in a robotic setup with sitting-drop vapor diffusion. Two conditions containing Mg^{2+} salts were further optimized in a manual plate setup with hanging-drop vapor diffusion to increase crystal size and quality. Note that in addition to the two protein containers, crystallization conditions contained a fixed amount of sodium chloride from the protein buffer whereas crystal growth was fine-tuned with varied amounts of magnesium salt. In this specific vapor diffusion setup, the total salt concentration in the crystallization drop and therefore the electrostatic screening between the two protein variants gently decreases over time until crystallization occurs. High-quality crystals with up to 200 μm edge length could be readily obtained within 1 day (Figure 2B).

The structure of the binary crystals was determined by X-ray crystallography to a resolution of 1.80 Å, using synchrotron radiation (Table S1). The refined structure shows that the crystals are composed of both variants, with a 1:1 stoichiometry (see Figure S4 for omit maps). To the best of our knowledge, this represents the first structure of two complementarily charged proteins derived from the same parent protein. The containers form a tetragonal lattice with unit cell parameters of a = 126.6 Å and c = 174.9 Å in space group $P4$ (Figure 2C and Table S1). In addition to contacts between oppositely charged containers, interactions between like-charged containers (Ftn$^{(neg)}$ with Ftn$^{(neg)}$ and Ftn$^{(pos)}$ with Ftn$^{(pos)}$) are present. In total, each container is coordinated by eight containers of opposite charge (cuboid coordination polyhedra), whereas it is also coordinated by four containers of the same charge (square-planar coordination), giving a coordination number of 12 for each container (Figure 2D). The contacts between containers take place close to the twelve 2-fold symmetry axes of each ferritin container. For each type of contact, a different set of residues is recruited to form hydrogen bonds and salt bridges with the contact partner. This plasticity allows the maximization of the more favorable contacts between oppositely charged containers (larger number of side chain interactions, Figure S5A) while simultaneously permitting coordination between like-charged containers (Figure S5B,C). As a result, the distance between the centers of oppositely charged containers (12.52 nm) is shorter than the distance between like-charged containers (12.66 nm). According to Pauling's rules,[36] for oppositely charged ions with cation−anion radius ratio close to 1.0, a cubic CsCl-type structure would be expected, where attractive forces are maximized and repulsive forces minimized. However, in the present structure additional attractive interactions between like-charged containers complement the interactions between oppositely charged containers, surpassing the simple ionic interactions in inorganic salts. This results in shortening of two unit cell edges and elongation of the third one compared to the cubic CsCl structure type, giving rise to a tetragonal unit cell with a more tightly packed arrangement (Figure 2D).

The binary ferritin crystals shown here present a porous scaffold with well-ordered cavities and channels (crystal solvent content 55.3%). Prior to crystal formation, the protein container cavities can be used for the encapsulation of nanoparticles (Figure 1B). Subsequently, the protein−nanoparticles composites are assembled into a superlattice by applying the same crystallization conditions as for empty containers (Figure 1C). The binary nature of the crystals enables organization of two different types of nanoparticles: one type encapsulated into Ftn$^{(pos)}$ and the other one into Ftn$^{(neg)}$. Because the crystal contacts are solely formed between the protein containers, we expect the nanoparticle lattice to have the same tetragonal structure as the parent crystal.

As an application for the binary protein material, we chose to assemble inorganic nanoparticles into binary superlattices. To this end, we prepared composites of protein containers loaded with metal oxide nanoparticles. As cargo, we selected cerium oxide and cobalt oxide nanoparticles because of their potential application in catalysis and as components of magnetic materials.[37−39]

Cerium oxide nanoparticles were synthesized within the cavity of Ftn$^{(pos)}$ and cobalt oxide nanoparticles within Ftn$^{(neg)}$ in

DOI: 10.1021/jacs.6b07260
J. Am. Chem. Soc. 2016, 138, 12731−12734

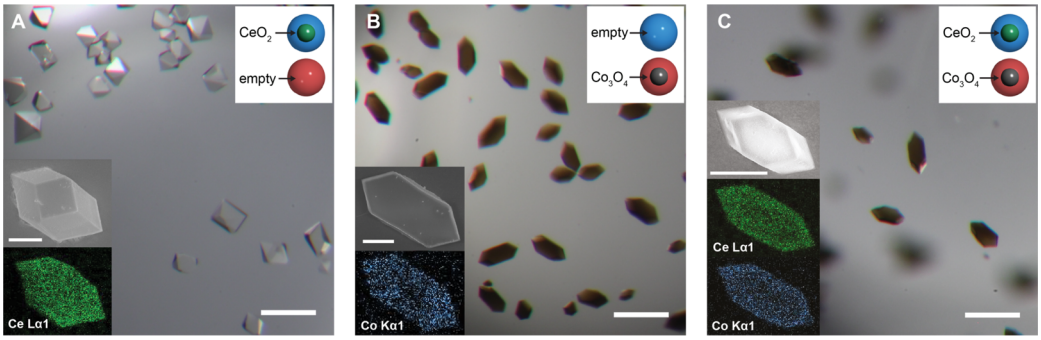

Figure 3. Optical microscopy images of binary protein−NP crystals in the crystallization condition. Inset shows the SEM image of a representative crystal (top) and the EDX mapping (bottom). Binary crystals composed of (A) $Ftn^{(pos)}$ CeO_2 and $Ftn^{(neg)}$ empty. (B) $Ftn^{(pos)}$ empty and $Ftn^{(neg)}$ Co_3O_4. (C) $Ftn^{(pos)}$ CeO_2 and $Ftn^{(neg)}$ Co_3O_4. Scale bar for optical microscopy images 200 μm, for SEM images 20 μm.

solution, following an adapted procedure.[30] In gel filtration chromatography, the protein container fractions have a strong absorbance above 350 nm indicative of the metal oxide nanoparticles coeluting with the protein container (Figure S6). Empty or weakly loaded protein containers were removed by density gradient centrifugation with a sucrose gradient to ensure high occupancy of nanoparticles in binary crystals. In negative stain TEM analysis, all variants show intact protein shells with a diameter of 12 nm similar to empty ferritin containers (Figures S7 and S8). Direct observation without stain confirmed that the nanoparticles are not exceeding the boundaries of the inner cavity size (~6−8 nm; Figures S7 and S8 and Table S2). The composition of the nanoparticle cores was further analyzed with electron diffraction: cobalt oxide nanoparticles were determined as Co_3O_4 (Figure S9 and Table S3) and cerium oxide nanoparticles as CeO_2 (Figure S10 and Table S4).

Nanoparticle-loaded protein containers were subjected to crystallization, applying the same conditions as for empty containers. We first tested crystals with only one variant loaded with nanoparticles (Figure 3A,B) before producing mixed crystals with both cerium and cobalt oxide nanoparticles (Figure 3C). For other combinations, including both variants loaded with the same nanoparticle type and variants loaded with iron oxide nanoparticles, refer to the SI. Figure 3 shows optical microscopy images of binary crystals of NP-loaded $Ftn^{(pos)}$ and $Ftn^{(neg)}$ with up to 150 μm edge length. To enhance the stability of the crystals, the protein shells were cross-linked with glutaraldehyde after crystal formation by simply adding the cross-linking agent to the reservoir solution. Cross-linked crystals could be readily manipulated, and washed in pure water and dried to yield free-standing crystals. Crystals were stable in SEM analysis in the electron beam under vacuum (Figure 3 inset). Applying energy dispersive X-ray spectroscopy (EDX mapping) clearly shows that the crystals contain the elements (Ce and Co) corresponding to the respective nanoparticle types (Figure 3 inset).

The crystalline samples were further analyzed by small-angle X-ray scattering (SAXS) to determine the superstructure of the nanoparticles. The samples give rise to centric diffraction rings, with strong Bragg peaks visible in the 2D SAXS (Figure 4), indicating a high long-range order and large domain size of the crystals. To ensure data collection of ensemble diffraction rather than from a few single crystals, the samples were rotated during data collection, similarly to X-ray powder diffraction analysis. The 1D SAXS data (black line in Figure 4) confirmed that all crystals are composed of one single phase, with the nanoparticles assembled in a primitive tetragonal lattice. On the basis of the peak positions of the first two reflections (001) and (100), unit cell

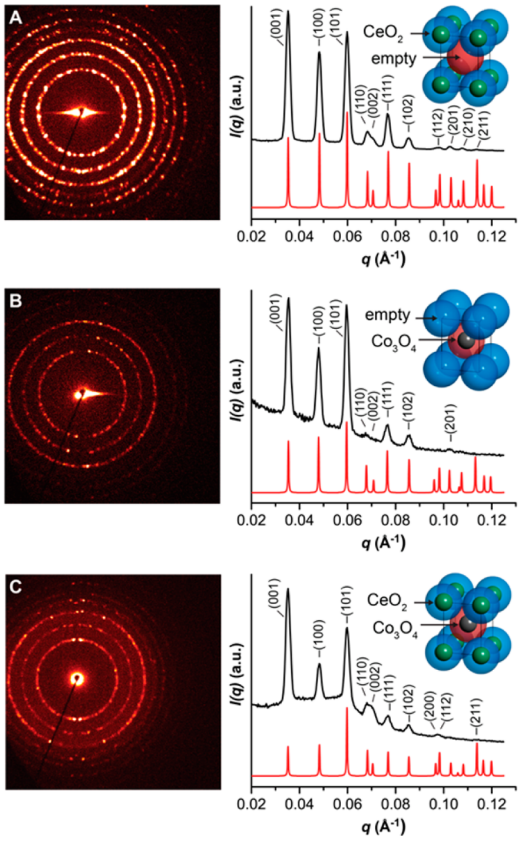

Figure 4. 2D and radially averaged 1D SAXS data for binary nanoparticle crystals (same samples as in Figure 3). Experimental data are shown in black, and simulated diffraction patterns in red. A unit cell of the corresponding crystal composition is shown.

parameters were derived and used to simulate the respective full diffraction patterns (red line in Figure 4), which coincide well with the experimental data. Notably, unit cell parameters were similar to crystals with empty containers (Figure S14) and independent from the nanoparticle cargo (mean values: a = 130.4 ± 0.5 Å, c = 178.1 ± 0.5 Å; Table S6).

This has important implications for the generation of superlattices based on protein containers: Because the protein container is the primary building block with a defined molecular envelope, the crystal lattice is solely defined by the protein shell and not the cargo particle. As a consequence, unrivaled long-range order and very large domain sizes of the nanoparticle superlattice could be achieved.

DOI: 10.1021/jacs.6b07260
J. Am. Chem. Soc. 2016, 138, 12731−12734

In summary, we produced binary superlattices of inorganic nanoparticles by exploiting electrostatic interactions between engineered protein containers. The assemblies consist of four different components: two oppositely charged protein containers with internal cavities, and two types of metal oxide nanoparticles within the cavities. These quaternary crystals demonstrate that protein containers with their atomically precise shell are well suited for the construction of nanoparticle superlattices with large assembly size. Free-standing crystals, substantial for future applications, could be obtained by facile in situ cross-linking. Importantly, the protein shell determines the structure of the assembly whereas functionality can be readily imparted by the choice of cargo, e.g., isotropic and anisotropic nanoparticles, enzymes, small molecules, or a combination of these. In combination with using differently sized protein shells for cargo assembly, multifunctional biohybdrid materials with tunable structures could be accessible.

■ ASSOCIATED CONTENT

Supporting Information

The Supporting Information is available free of charge on the ACS Publications website at DOI: 10.1021/jacs.6b07260.

Procedures (PDF), and data for 5JKL and 5JKM

■ AUTHOR INFORMATION

Corresponding Author

*tobias.beck@ac.rwth-aachen.de

Notes

The authors declare the following competing financial interest(s): T.B. and M.K. have filed a patent application concerning the use of binary protein crystals for the assembly of inorganic nanoparticles.

■ ACKNOWLEDGMENTS

We thank Birgit Hahn for SEM data collection, Dr. Riza Iskandar and Tobias Caumanns for support during TEM data collection, Prof. Ulrich Schwaneberg for generous support with regard to protein production, Prof. Walter Richtering for SAXS access, Prof. Fitter for access to a crystallization robot, and Prof. Ulrich Simon for general support and helpful discussions. Plasmid containing $Ftn^{(pos)}$ was a kind gift of Prof. Donald Hilvert. This work was generously supported by a Liebig scholarship to T.B. (Fonds der Chemischen Industrie), a doctoral scholarship to M.K. (Fonds der Chemischen Industrie), the DFG, and a RWTH Startup grant (funded by the Excellence Initiative of the German federal and state governments) to T.B.

■ REFERENCES

(1) Tseng, R. J.; Tsai, C.; Ma, L.; Ouyang, J.; Ozkan, C. S.; Yang, Y. *Nat. Nanotechnol.* **2006**, *1*, 72−77.

(2) Zheng, J.; Constantinou, P. E.; Micheel, C.; Alivisatos, A. P.; Kiehl, R. A.; Seeman, N. C. *Nano Lett.* **2006**, *6*, 1502−1504.

(3) Miao, L.; Han, J.; Zhang, H.; Zhao, L.; Si, C.; Zhang, X.; Hou, C.; Luo, Q.; Xu, J.; Liu, J. *ACS Nano* **2014**, *8*, 3743−3751.

(4) Park, S. Y.; Lytton-Jean, A. K. R.; Lee, B.; Weigand, S.; Schatz, G. C.; Mirkin, C. *Nature* **2008**, *451*, 553−556.

(5) Nykypanchuk, D.; Maye, M. M.; van der Lelie, D.; Gang, O. *Nature* **2008**, *451*, 549−52.

(6) Macfarlane, R. J.; Jones, M. R.; Lee, B.; Auyeung, E.; Mirkin, C. A. *Science* **2013**, *341*, 1222−1225.

(7) Tian, Y.; Zhang, Y.; Wang, T.; Xin, H. L.; Li, H.; Gang, O. *Nat. Mater.* **2016**, *15*, 654−661.

(8) Sinclair, J. C.; Davies, K. M.; Vénien-Bryan, C.; Noble, M. E. M. *Nat. Nanotechnol.* **2011**, *6*, 558−562.

(9) Lanci, C. J.; Macdermaid, C. M.; Kang, S.-g.; Acharya, R.; North, B.; Yang, X.; Qiu, X. J.; Degrado, W. F.; Saven, J. G. *Proc. Natl. Acad. Sci. U. S. A.* **2012**, *109*, 7304−7309.

(10) Brodin, J. D.; Ambroggio, X. I.; Tang, C.; Parent, K. N.; Baker, T. S.; Tezcan, F. A. *Nat. Chem.* **2012**, *4*, 375−382.

(11) Sontz, P. A.; Bailey, J. B.; Ahn, S.; Tezcan, F. A. *J. Am. Chem. Soc.* **2015**, *137*, 11598−11601.

(12) Shenton, W.; Davis, S. A.; Mann, S. *Adv. Mater.* **1999**, *11*, 449−452.

(13) McMillan, R. A.; Paavola, C. D.; Howard, J.; Chan, S. L.; Zaluzec, N. J.; Trent, J. D. *Nat. Mater.* **2002**, *1*, 247−252.

(14) Hu, M.; Qian, L.; Briñas, R. P.; Lymar, E. S.; Hainfeld, J. F. *Angew. Chem., Int. Ed.* **2007**, *46*, 5111−5114.

(15) Sun, J.; DuFort, C.; Daniel, M.-C.; Murali, A.; Chen, C.; Gopinath, K.; Stein, B.; De, M.; Rotello, V. M.; Holzenburg, A.; Kao, C. C.; Dragnea, B. *Proc. Natl. Acad. Sci. U. S. A.* **2007**, *104*, 1354−9.

(16) Wei, H.; Wang, Z.; Zhang, J.; House, S.; Gao, Y.-G.; Yang, L.; Robinson, H.; Tan, L. H.; Xing, H.; Hou, C.; Robertson, I. M.; Zuo, J.-M.; Lu, Y. *Nat. Nanotechnol.* **2011**, *6*, 93−97.

(17) Kostiainen, M. A.; Hiekkataipale, P.; Laiho, A.; Lemieux, V.; Seitsonen, J.; Ruokolainen, J.; Ceci, P. *Nat. Nanotechnol.* **2013**, *8*, 52−56.

(18) Brodin, J. D.; Auyeung, E.; Mirkin, C. A. *Proc. Natl. Acad. Sci. U. S. A.* **2015**, *112*, 4564−4569.

(19) Shevchenko, E. V.; Talapin, D. V.; Kotov, N. A.; O'Brien, S.; Murray, C. B. *Nature* **2006**, *439*, 55−59.

(20) Cheon, J.; Park, J.-I.; Choi, J.-s.; Jun, Y.-w.; Kim, S.; Kim, M. G.; Kim, Y.-M. J.; Kim, Y.-M. J. *Proc. Natl. Acad. Sci. U. S. A.* **2006**, *103*, 3023−3027.

(21) King, N. P.; Sheffler, W.; Sawaya, M. R.; Vollmar, B. S.; Sumida, J. P.; André, I.; Gonen, T.; Yeates, T. O.; Baker, D. *Science* **2012**, *336*, 1171−1174.

(22) Lai, Y.-T.; Reading, E.; Hura, G. L.; Tsai, K.-L.; Laganowsky, A.; Asturias, F. J.; Tainer, J. A.; Robinson, C. V.; Yeates, T. O. *Nat. Chem.* **2014**, *6*, 1065−1071.

(23) Seebeck, F. P.; Woycechowsky, K. J.; Zhuang, W.; Rabe, J. P.; Hilvert, D. *J. Am. Chem. Soc.* **2006**, *128*, 4516−4517.

(24) Butts, C. A.; Swift, J.; Kang, S.-G.; Di Costanzo, L.; Christianson, D. W.; Saven, J. G.; Dmochowski, I. J. *Biochemistry* **2008**, *47*, 12729−12739.

(25) Hommersom, C. A.; Matt, B.; van der Ham, A.; Cornelissen, J. J. L. M.; Katsonis, N. *Org. Biomol. Chem.* **2014**, *12*, 4065−4069.

(26) Wörsdörfer, B.; Woycechowsky, K. J.; Hilvert, D. *Science* **2011**, *331*, 589−592.

(27) Abe, S.; Hirata, K.; Ueno, T.; Morino, K.; Shimizu, N.; Yamamoto, M.; Takata, M.; Yashima, E.; Watanabe, Y. *J. Am. Chem. Soc.* **2009**, *131*, 6958−6960.

(28) Clegg, G.; Fitton, J. E.; Harrison, P. M.; Treffry, A. *Prog. Biophys. Mol. Biol.* **1980**, *36*, 56−86.

(29) Wong, K. K. W.; Mann, S. *Adv. Mater.* **1996**, *8*, 928−932.

(30) Uchida, M.; Flenniken, M. L.; Allen, M.; Willits, D. A.; Crowley, B. E.; Brumfield, S.; Willis, A. F.; Jackiw, L.; Jutila, M.; Young, M. J.; Douglas, T. *J. Am. Chem. Soc.* **2006**, *128*, 16626−16633.

(31) Klem, M. T.; Mosolf, J.; Young, M.; Douglas, T. *Inorg. Chem.* **2008**, *47*, 2237−2239.

(32) Yang, Z.; Wang, X.; Diao, H.; Zhang, J.; Li, H.; Sun, H.; Guo, Z. *Chem. Commun.* **2007**, 3453−3455.

(33) Liu, G.; Wang, J.; Lea, S. A.; Lin, Y. *ChemBioChem* **2006**, *7*, 1315−1319.

(34) Hennequin, B.; Turyanska, L.; Ben, T.; Beltrán, A. M.; Molina, S. I.; Li, M.; Mann, S.; Patanè, A.; Thomas, N. R. *Adv. Mater.* **2008**, *20*, 3592−3596.

(35) Beck, T.; Tetter, S.; Künzle, M.; Hilvert, D. *Angew. Chem., Int. Ed.* **2015**, *54*, 937−940.

(36) Pauling, L. *J. Am. Chem. Soc.* **1929**, *51*, 1010−1026.

(37) Xu, C.; Qu, X. *NPG Asia Mater.* **2014**, *6*, e90.

(38) Dong, J.; Song, L.; Yin, J. J.; He, W.; Wu, Y.; Gu, N.; Zhang, Y. *ACS Appl. Mater. Interfaces* **2014**, *6*, 1959−1970.

(39) Skumryev, V.; Stoyanov, S.; Zhang, Y.; Hadjipanayis, G.; Givord, D.; Nogues, J. *Nature* **2003**, *423*, 850−853.

DOI: 10.1021/jacs.6b07260
J. Am. Chem. Soc. 2016, 138, 12731−12734